Lab on a Chip

PAPER

View Article Online
View Journal | View Issue

Cite this: *Lab Chip*, 2015, **15**, 3086

UV-nanoimprint lithography as a tool to develop flexible microfluidic devices for electrochemical detection

Juhong Chen,†[a] Yiliang Zhou,†[b] Danhui Wang,[a] Fei He,[a] Vincent M. Rotello,[c] Kenneth R. Carter,[b] James J. Watkins[b] and Sam R. Nugen*[a]

Received 6th May 2015,
Accepted 12th June 2015

DOI: 10.1039/c5lc00515a

www.rsc.org/loc

Research in microfluidic biosensors has led to dramatic improvements in sensitivities. Very few examples of these devices have been commercially successful, keeping this methodology out of the hands of potential users. In this study, we developed a method to fabricate a flexible microfluidic device containing electrowetting valves and electrochemical transduction. The device was designed to be amenable to a roll-to-roll manufacturing system, allowing a low manufacturing cost. Microchannels with high fidelity were structured on a PET film using UV-NanoImprint Lithography (UV-NIL). The electrodes were inkjet-printed and photonically sintered on second flexible PET film. The film containing electrodes was bonded directly to the channel-containing layer to form sealed fluidic device. Actuation of the multivalve system with food dye in PBS buffer was performed to demonstrate automated fluid delivery. The device was then used to detect *Salmonella* in a liquid sample.

Introduction

Multiple materials such as glass, silicon, plastic, paper, hydrogels, polymer and composite materials have been used to fabricate microfluidic devices.[1] Recently, significant emphasis has been placed on low-cost biosensors for use in low-resource settings such as sub-Saharan Africa or remote parts of South America and Southeast Asia.[2–5] While many researchers have now focused their attention on inexpensive materials to produce low-cost devices,[2,3,6,7] the method of fabrication must also be taken into account during design to provide truly low-cost production.

Among the materials used for microfluidic devices, polymers possess several attractive features such as low cost, biocompatibility, and disposability. Several fabrication techniques have been developed for polymer microfluidic devices, such as laser ablation, hot embossing and polymer casting.[8,9] As a result, several examples of polymer microfluidic devices have been developed for use in clinical diagnosis, food safety, and environmental monitoring.[10,11]

Polymeric materials, such as cyclic olefin copolymer (COC), polycarbonate (PC), polyvinyl chloride (PVC), poly(methyl methacrylate) (PMMA) and polydimethylsiloxane (PDMS) have been commonly reported as substrates for microfluidic devices.[12] Of all of the above-mentioned polymeric materials, PDMS is the most common choice due to its simple fabrication, low cost, gas permeability, optical transparency, and non-toxicity.[12] Despite the convenience of PDMS and broad usage in academic laboratories, several drawbacks have limited the application of PDMS microchips: (1) poor chemical compatibility with many organic solvents; (2) surface modifications of PDMS are unstable over time; (3) the ability of PDMS to absorb small molecules into its matrix.[12] To overcome these concerns with PDMS microchips, Carlborg *et al.* reported a novel polymer microfluidic platform using thiol-ene (TE) polymer-based soft lithography.[13] Saharil *et al.* also have introduced "click chemistry" using TE polymers to generate microchips rapidly with high purity and high yield.[14]

To date, very few examples of these soft material microfluidic devices have been fabricated by high-throughput means, with even fewer demonstrating commercial success. In our study, we used UV curable TE polymers and PET films to form a flexible microfluidic chip *via* nanoimprint lithography (NIL). NIL can be applied to roll-to-roll processing on a large-scale fabrication system allowing for high throughput and low-cost.[15] The roll-to-roll fabrication system allows for continuous processing on inexpensive flexible polymer substrates such as polyethylene terephthalate (PET) film. NIL allows the microfluidic channels to be continuously formed on the flexible films with high fidelity. The roll-to-roll

[a] *Department of Food Science, University of Massachusetts, 102 Holdsworth Way, Amherst, MA 01003, USA. E-mail: snugen@umass.edu*
[b] *Department of Polymer Science and Engineering, University of Massachusetts, 120 Governors Drive, Amherst, MA 01003, USA*
[c] *Department of Chemistry, University of Massachusetts, 710 North Pleasant Street, Amherst, MA 01003, USA*
† These authors have contributed equally to this work.

microfluidic fabrication process will open up a high volume manufacturing and low cost platform for the future fabrication of microfluidic sensors.[16]

Although many microfluidic devices are highly sensitive and specific, most require an additional external pumping mechanism to operate, which limits their true portability and utility in point-of-care setting. Thus, some alternative methods such as electroosmotic flow have been developed to transport fluid.[17] Electroosmotic flow, however, requires a high voltage source and is therefore less practical in a portable device. In contrast, the use of capillary flow to transport solutions does not require an external pump and can therefore simplify device design and fabrication, *e.g.* in pregnancy and blood sugar tests.[18] The capillary flow within a microchannel is governed by several factors including the channel dimensions, sample viscosity, surface tension and contact angle between the sample and microchannel wall.[19] If the substrate selected for the microchannel cannot provide adequate capillary flow, reduction of the contact angle through surface modification must be considered. Oxygen plasma[20] or UV irradiation[21,22] are commonly used to create a hydrophilic surface, and thus improve capillary flow.

Metal evaporation or sputter coating coupled with photolithography is considered standard practice for the fabrication of metalized electrode arrays in microfluidic devices.[23,24] Comparatively, inkjet-printing can be used for high throughput, low-cost and continuous fabrication processes without the need for metal removal. This method also offers the advantage of small feature sizes, rapid prototyping and targeted patterning. Inkjet-printed electrodes have been demonstrated for use as electrowetting valves in microfluidics.[21,22,25,26] Electrowetting on dielectric (EWOD) is a phenomenon where the hydrophobicity of a dielectric can be shifted to hydrophilic if a potential is applied across the electrode.[27] For example, hydrophobic polytetrafluoroethylene (PTFE), which is commonly used for electrowetting, becomes polarized and therefore hydrophilic when a potential is applied. Therefore, an electrowetting PTFE layer, which can shift contact angle, can act as an electronically-controlled valve within a microchannel without the need of moving parts or an external pump.[25] In addition to surface engineering, the utility of microfluidic devices can be greatly enhanced through fluid handling valves.

In this paper, we created a low-cost, pump-free, capillary flow-driven microfluidic chip that can control the flow of solutions in the microchannel, as well as demonstrated the utility of the device for electrochemical detection. The fabrication process used photolithography to fabricate an SU-8 master and thermal curing to make a PDMS stamping template for nanoimprint lithography. The final device consisted of two flexible PET layers combined to form a flexible microfluidic device. One layer containing microchannels was formed using a UV curable TE polymer based on nanoimprint lithography. The inkjet-printed three-electrode system and electrowetting valves were located on the opposing layer (Fig. 1). A key feature of this strategy is that all processes can be scaled up to a roll-to-roll system to produce biosensors at a high throughput and low cost.

Materials and methods

SU-8 master and PDMS template

The microchannel pattern was fabricated on a 5 inch silicon wafer using standard photolithography. Briefly, SU-8 2015 photoresist (MicroChem, Westborough, MA) was deposited onto the center of the silicon wafer and spun for 5 seconds at 500 rpm followed by 1 minute at 1000 rpm. The final thickness of resist was approximately 55 μm. The SU-8 structures were patterned using a contact aligner (Karl SUSS MA6, SUSS MicroTec, Garching, Germany) following a soft bake at 95 °C for 4 minutes on a level hotplate. After developing for 4 min in SU-8 developer with gentle agitation, a post exposure bake of 95 °C for 5 minutes was performed. The wafer was then washed with isopropanol alcohol and dried with nitrogen gas. Finally, the patterned wafer was baked at 95 °C for 2 minutes and stored until use. The PDMS elastomer mixture (10 : 1 weight ratio of Sylgard 184 silicone elastomer base and curing agent, Dow Corning) was mixed and degassed in vacuum oven for 1 hour at room temperature. The mixture was then poured on the SU-8 patterned wafer and placed into a heated oven. After heating at 60 °C for 2 hours, the PDMS template was carefully removed from the master wafer. The dimensions of the SU-8 master and PDMS template were measured by optical profilometry (Zeta Instruments, San Jose, CA).

UV-nanoimprinting of microfluidic channels

The nanoimprint resist consisted of 2.40 g of 1,3,5-triallyl-1,3,5-triazine-2,4,6(1*H*,3*H*,5*H*)-trione (TE-allyl, Acros Organics, Fair Lawn, NJ), 3.60 g of pentaerythritol tetrakis(3-mercaptopropionate) (TE-thiol, Sigma-Aldrich, St. Louis, MO) and 0.06 g of benzoin methyl ether (Sigma-Aldrich, St. Louis, MO). The resist was spin-coated onto clean polyethylene terephthalate film (PET, 130 μm, McMaster, Robbinsville, NJ) at 500 rpm for 30 seconds. The nanoimprinting of microfluidic channels was performed using a Nanonex NX-2000 nanoimprinter (Nanonex, Monmouth Junction, NJ) using the PDMS template as a stamp. Nanoimprinting was conducted using UV light (365 nm) with a pressure of 482 kPa for 4 minutes.

Inkjet printing of electrodes

The electrode pattern was designed using AutoCAD (Autodesk, San Francisco, CA). The silver ink (JS-B30G, Novacentrix, Austin, TX) and gold ink (UTDAuIJ, UT Dots, Champaign, IL) were printed on a clean PET film using a Dimatix Inkjet Materials Printer (FujiFilm, Santa Clara, CA). For the deposition of both inks, the temperature of stage and printer head were set to 30 °C. The drop space was 30 μm, which provides a print resolution of 847 dpi. The driving voltage of the nozzles was 24–26 V. After printing, the silver and

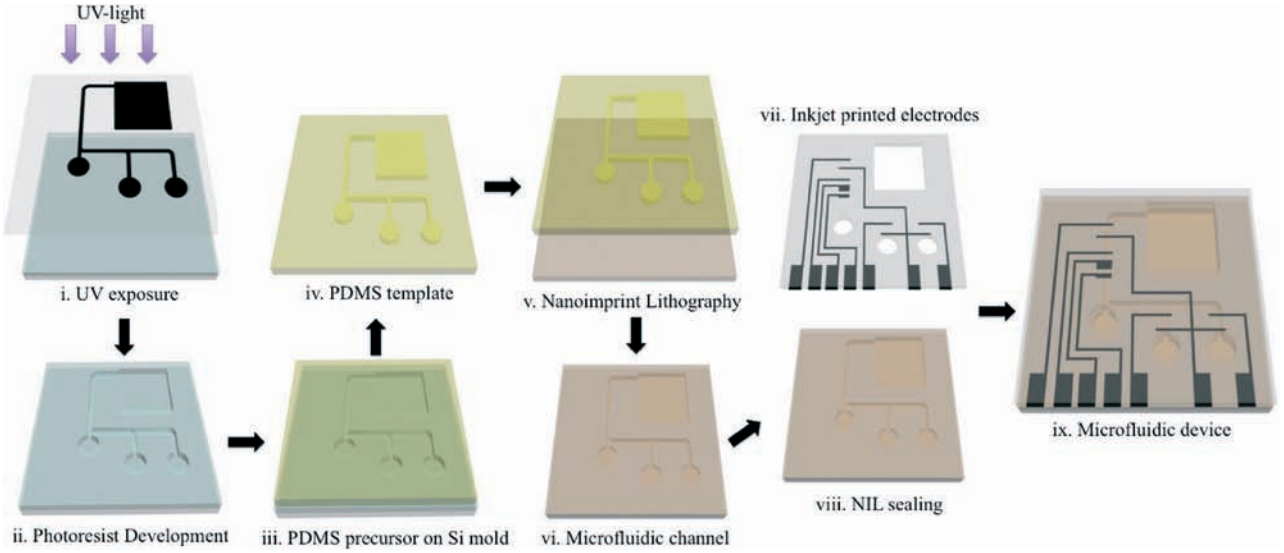

Fig. 1 Bonding of inkjet-printed electrodes and microfluidic channels to form a microfluidic device using nanoimprint lithography. (i) Spin coat SU-8 resist on silicon wafer and conduct photolithography (ii) remove the uncross-linked SU-8 resist using SU-8 development solution, (iii) pour PDMS oligomers on SU-8 master and thermal cure, (iv) replicated PDMS template, (v–vi) prepare microfluidic channels on flexible PET film using nanoimprint lithography, (vii) inkjet printed electrodes on flexible PET film, (viii) seal microfluidic channels and inkjet printed electrodes using nanoimprint lithography and (ix) microfluidic device.

gold electrodes were sintered using photonic curing (Novacentrix, Austin, TX) with 300 V/250 microseconds and 450 V/250 microseconds, respectively. In order to cut sample injection ports, the flexible PET film was laser ablated using a CO_2 laser (EpilogLaser, Golden, CO).

Electrowetting valve fabrication

The electrowetting valves required a hydrophobic surface modification on the second electrode. To modify these electrodes, 3 μL of 3 mM 1*H*,1*H*,2*H*,2*H*-perfluorodecanethiol (PFDT, Sigma-Aldrich, St. Louis, MO) in ethanol (Sigma-Aldrich, St. Louis, MO) was deposited on the second silver electrode of each valve. Following vaporization of the solution, the process was repeated three times to form a self-assembled monolayer (SAM).[25] The surface morphology of the electrodes was observed using Scanning Electron Microscopy (SEM, FEI Hillsboro, OR). Contact angles of electrodes before and after modification were measured using VCA Optima surface analysis/goniometry (AST Products, Billerica, MA).

Bonding process

A 5× diluted nanoimprint resist with propylene glycol monomethyl ether acetate (PGMEA, Alfa Aesar, Ward Hill, MA) was used for binding the PET film containing the microfluidic structures to another PET film containing the inkjet-printed electrodes. The binding resist was spin coated on PET film with microchannel at 2500 rpm for 30 seconds and placed on hot plate at 60 °C for 2 minutes. The PET containing inkjet-printed electrodes was aligned onto the channel-containing PET. Then, the Nanonex NX-2000 nanoimprinter was used to press the two films together under the UV light with a pressure of 172 kPa for 4 minutes.

Electrode characterization

All electrochemical measurements were conducted on the microfluidic chip using a handheld potentiostat (PalmSens, BV, Netherlands). Cyclic voltammetry (CV) was performed on the gold working electrode at room temperature between −0.5 V and +0.3 V using 1 mM ferrocene methylalcohol (Sigma-Aldrich, St. Louis, MO) in 0.05 M H_2SO_4. The CV was used to characterize the electrodes at various scan rates (5, 10, 25, 50, 100 and 200 mV s^{-1}).

Salmonella detection

Salmonella enterica (SA, ATCC 14028) was selected to demonstrate that the microfluidic device could be used to detect bacteria. The *Salmonella* was inoculated into Luria broth and incubated overnight at 37° at 200 rpm. The harvested bacteria were ten-fold serially diluted using 0.01 M phosphate buffer saline (PBS) buffer. 100 μL of diluted solution was plated on LB agar to obtain bacteria concentration. To perform the assay, 20 μL of antibody-conjugated magnetic beads (MB-Ab_1, Dynabeads®, Invitrogen™, Life Technologies) were added into 1 mL of a *Salmonella*-containing solution (10^5 and 10^6 CFU mL^{-1}, 0 CFU mL^{-1} as control), and agitated at room temperature for 30 minutes. The MB-Ab_1-SA were separated and washed three times using 0.01 M PBS buffer containing 1% bovine serum albumin (Fisher Scientific, Fair Lawn, NJ), and dispersed into 1 mL of PBS buffer. 20 μL of 10 μg mL^{-1} alkaline phosphatase labelled antibody (ALP-Ab_2, KPL, MD) were added into above solutions and incubated for 30 minutes at room temperature. After placing magnet under the working electrode, 10 μL of the sample solutions, washing buffer and enzymatic substrate solution containing 5 mM L-ascorbic acid 2-phosphate (AAP, Fisher Scientific, St. Louis,

MO) and 10 mM tris(2-carboxyethyl)phosphine (TCEP, Fisher Scientific, St. Louis, MO) were pipetted into inlet 1, inlet 2 and inlet 3, respectively. Following a 30 minute incubation, the electrowetting valves were opened in a timed series and amperometric detection (condition: potential: 0.35 V; scan rate: 0.01 mV s^{-1}; time: 150 second) was conducted to quantify the analyte.

Results and discussion

SU-8 mater and PDMS template characterization

Photolithography using SU-8 is a common method to fabricate micro-scale molds for microfluidics.[28] A thickness below 2 μm was obtained by diluting the resist. In this study, an SU-8 structured wafer was used as a mold for the PDMS template (stamp). After PDMS oligomers were poured on the SU-8 master and cured, PDMS could be removed from the master without disruption of the formed structures. This method has previously been used to replicate submicron feature sizes in PDMS.[29] The replicated features of microchannel were measured using optical profilometry. The profilometry results for both the SU-8 master and PDMS template were shown in Fig. 2. For the microfluidic channel design, the microchannels were 1000 μm in the width and 55 μm in depth (Fig. 2c and d).

Inkjet-printed electrode characterization

Electrodes for microfluidic devices are commonly patterned using either photolithographic methods that involves the sputtering or evaporating of metals,[30] or screen printing where a conductive paste is patterned through a mesh.[31] While photolithographic methods can offer exceptional feature sizes, the process is expensive, requires a vacuum, and therefore is not always applicable for high throughput, low-cost devices. Inkjet-printing of electrodes provides the advantage of rapid prototyping and targeted patterning. Inkjet-printing has also previously been paired with roll-to-roll manufacturing for continuous processing.[32]

In our current study, the working electrode and counter electrode pads (gold nanoparticle ink) and the valves and reference electrode (silver nanoparticle ink) were inkjet-printed on flexible PET film using Fuji Dimatix Inkjet Materials Printer (Fig. 3a). The inks all required high temperature sintering for adequate electrical conductivity. Compared to microwave flash sintering,[33] laser pulse sintering[34] and oven-based sintering at high temperatures, a sintering process using UV photonic curing allowed the use of PET as a substrate that has a lower temperature tolerance. The UV photonic curing provided an instantaneous high temperature to evaporate the solvents and surfactants in the inks and sinter the nanoparticles for improved conductivity. Fig. 3b shows the gold electrodes (i and ii) and silver electrodes (iii and iv), respectively, before and after photonic sintering. After sintering, the sample injection ports on the PET film containing electrodes were cut using a CO_2 laser (Fig. 3c). The morphology of inkjet printed electrodes on flexible PET film was measured using SEM at varying magnifications (Fig. 3d–f).

Contact angle measurements

The most important influencing factor of capillary flow within a microchannel is contact angle (hydrophilicity) of the

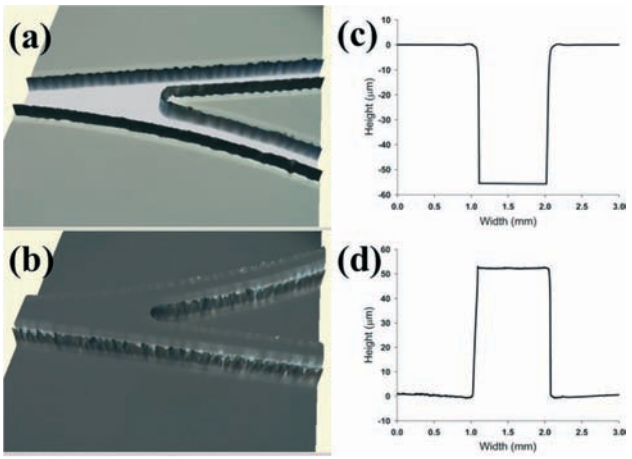

Fig. 2 Optical 3D profilometry images of (a) SU-8 master and (b) PDMS template, channel thickness of (c) SU-8 master and (d) PDMS template.

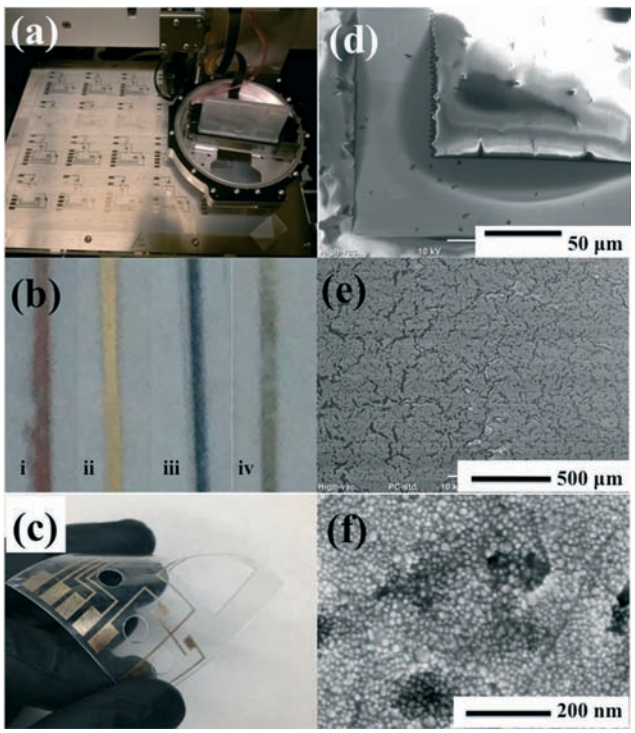

Fig. 3 Photography of (a) electrodes were inkjet-printed by inkjet printer, (b) inkjet-printed gold electrode (i and ii) and silver electrode (iii and iv) before and after sintering using Pulseforge, respectively, (c) electrodes on flexible PET film, (d–f) SEM images of electrode on flexible PET film at different magnifications.

channel surface in addition to some properties of the liquid. Water contact angle measurements provide a quantitative measure of wettability, with hydrophobic surfaces having a large contact angle >90°. In our study, all the contact angles on solid surfaces were measured using 10 μL PBS buffer (0.01 M, pH 7.4) on a VCA Optima Goniometer (AST Products, Billerica, MA). PDMS is hydrophobic by nature. Oxygen plasma treatment can decrease the contact angle and yield a hydrophilic surface. However the surface wettability will be affected as the surface reverts to be hydrophobic in nature within several hours to a few days, depending on temperature.[35] The UV curable TE polymer we used in our study can overcome this issue. The contact angles of UV curable TE polymer and PET film were 77.8° ± 2.1 (Fig. 4a) and 77.4° ± 1.5 (Fig. 4b), respectively. The use of these polymers provides a suitable hydrophilicity for a capillary-driven microfluidic device.

In contrast to the channels, hydrophobic surfaces are required for electrowetting valves. The contact angle of bare silver electrode was 76.1° ± 5.3 (Fig. 4c). Following surface modification with 1*H*,1*H*,2*H*,2*H*-perfluorodecanethiol (PFDT), contact angle of silver electrodes increased to 134.2° ± 0.2 (Fig. 4d), which acts as a barrier for capillary flow. A reduction in contact angle using the electrowetting process allows the capillary flow to continue.

Surface morphology of the microchannel

In our study, the main compounds of UV curable TE precursor were 1,3,5-triallyl-1,3,5-triazine-2,4,6(1*H*,3*H*,5*H*)-trione (TE-allyl) and pentaerythritol tetrakis(3-mercaptopropionate) (TE-thiol) (Fig. 5a). Under UV irradiation, the precursor cross-linked and solidified through bonding between a carbon double bond and thiol group.[36,37] In order to fabricate the microchannel, a thin layer of TE precursor was spin coated on a PET film. After pattern-containing PDMS stamp was placed on the PET, the TE conformed to the stamp and was cross-linked with UV light. After the microchannel was hardened, the PDMS template was removed and the microchannel structure was obtain on flexible PET film (Fig. 5b).

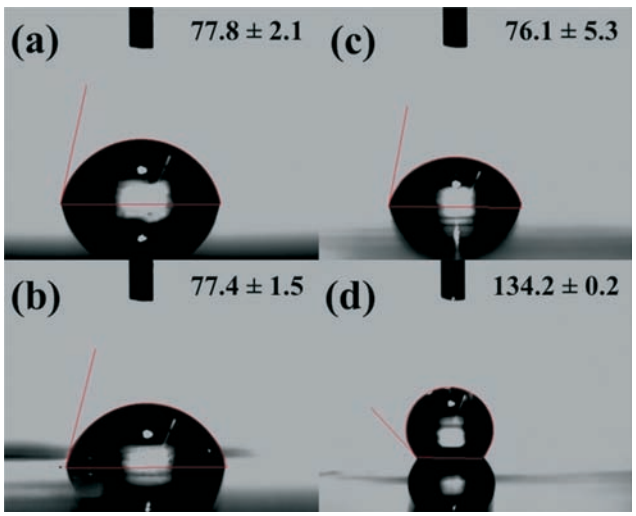

Fig. 4 Contact angles of 10 μL of PBS buffer on (a) TEs polymers, (b) PET film, (c, d) silver electrode before and after surface modification, respectively.

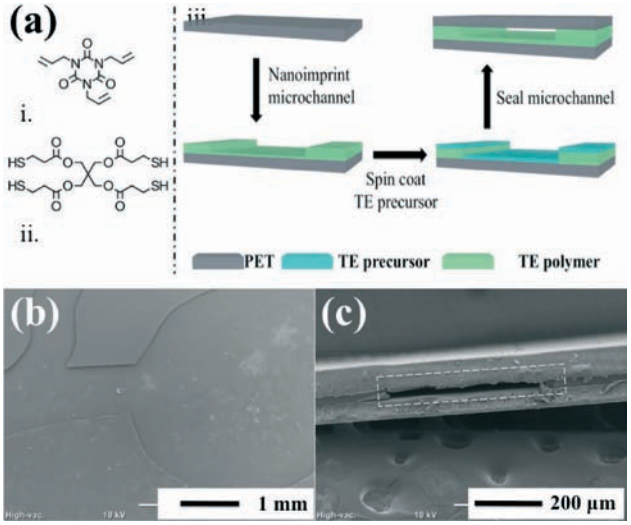

Fig. 5 (a) TE polymer precursor (i) TE-allyl, (ii) TE-thiol, (iii) diagram of bonding process using nanoimprint lithography, (b) SEM images of microfluidic channel on flexible PET film and (c) cross-sectional SEM image of a sealed microchannel.

Following the surface modification of the electrowetting electrodes, the electrode-structured PET films and the microchannel-structured PET films were bonded together to seal the fluidic device. The bonding process was likewise accomplished using nanoimprint lithography (Fig. 5a). Firstly, a thin coating of 5× diluted TE precursor was deposited onto the PET film containing the microchannels. This film was then aligned onto the electrode-containing PET and pressed together. The three layers (PET film-TE polymer-PET film) can been observed on a cross-sectional image of a sealed microchannel (Fig. 5c).

Electrowetting valve actuation

In our previous reports, we have described electronic valves that have been implanted into capillary flow microfluidic devices.[21,25,26] These electronic valves, which function on the principle of electrowetting, were able to be actuated at a low-voltage. Each electrowetting valve contained two inkjet-printed silver electrodes. The second electrode modified with hydrophobic monolayer (PFDT) resulted in a termination of capillary flow. He *et al.* reported that a potential of 4 V can reduce water contact angle to 70° within 10 seconds which allowed capillary flow to continue.[25] Koo *et al.* inkjet printed silver electrodes on paper-based analytical device to control the flow of reagents.[26]

In our work, a pump-free microfluidic chip using UV curable flexible polymer film has been developed. The fluid delivery is driven by capillary flow and incorporated an

absorbent pad for continuous flow. In order to test the performance of electrowetting, food dyes in 0.01 M phosphate buffer saline solution were used for visual help. The flow of all three dye solutions was stopped at the second silver electrodes that were modified with PFDT (Fig. 6b). To actuate the valves, a 12 V potential was applied across the modified and unmodified electrodes. This application of potential resulted in the continuation of capillary flow within the channel (Fig. 6c–e). The solutions were delivered across the working electrodes at specific time intervals and orders (yellow, red, green). This format enables a simple automation of the assay procedure using a standard relay.

Characterization of electrochemical microchip

The three-electrode system on the microfluidic chip was designed to conduct an electrochemical detection on-chip. In order to facilitate the transfer of charge from analyte, the surface area of working electrode was inkjet printed larger than other two electrodes. In our study, a standard Ag/AgCl electrode was selected as the reference electrode. To fabricate the electrode on the film, KCl (3.5%, w/v) was deposited onto the reference electrode and the electrodes were then baked at 95 °C for 5 minutes. This process was repeated three times.[38] Cyclic voltammetry on the gold working electrodes were run in triplicate using 10 μL of 1 mM ferrocene methylalcohol in 0.05 M H_2SO_4 to demonstrate the electrode functionality. Six scan rates (5, 10, 25, 50, 100 and 200 mV s^{-1}) were tested from −0.5 V to +0.3 V at potential step of 0.01 V. The characteristic volatmmograms as a function of scan rate are shown in Fig. 7. The anodic and cathodic peak currents were plotted to the square root of the scan rate between 5 to 200 mV s^{-1} (inserted figure). The current on gold working electrode exhibited a linear relation to the square root of the scan rate, which agreed with the Randels–Sevick relation.[39] The linear relation indicated the mass transfer in this three-electrode system was a diffusion-controlled process similar to reported electrodes.[40,41]

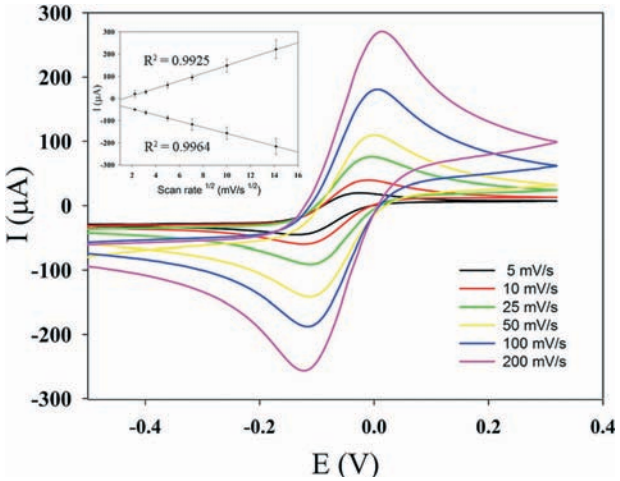

Fig. 7 Representative cyclic voltammetry of gold working electrode at different scan rate (5, 10, 25, 50, 100 and 200 mV s^{-1}) for 1 mM ferrocene methylalcohol in 0.05 M H_2SO_4. All of the CVs were detected under the same potential step from −0.5 V to +0.3 V, (insert figure) the relationship between anodic and cathodic currents and the square root of the scan rate, each measurement was carried out in triplicates using a new microchip (n = 3).

Salmonella detection

Salmonella is a pathogen often associated with contaminated food or water.[42–44] The ability to rapidly detect *Salmonella* in

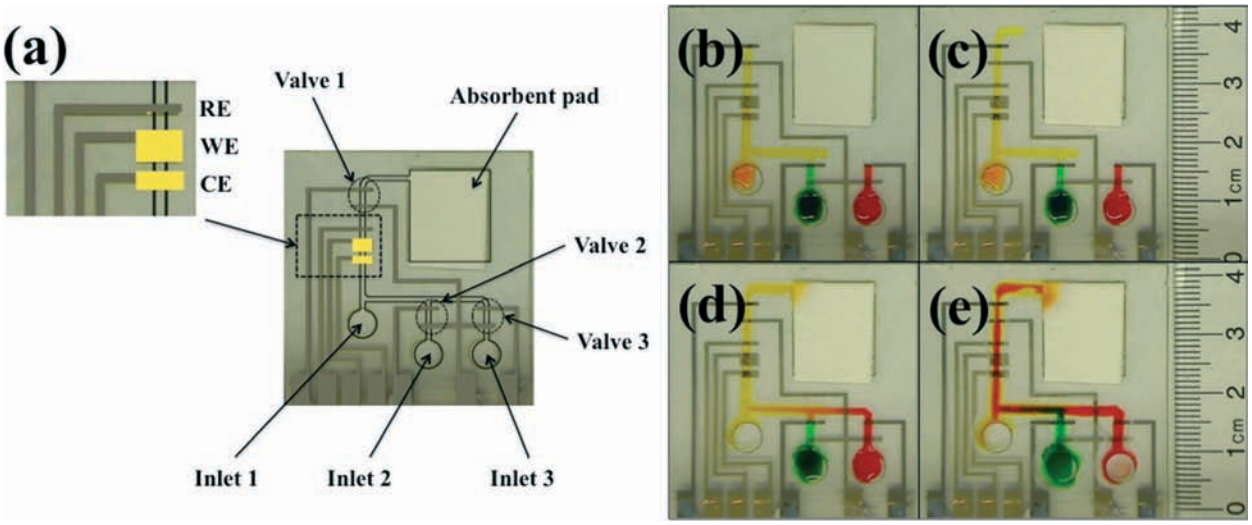

Fig. 6 (a) Schematic diagram of microfluidic chip consisting of three inlets, three electrode valves and three electrode system. RE: reference electrode; WE: working electrode; CE: counter electrode, visual inspection of electrowetting on microfluidic chip using food dye solution (0.01 M phosphate-buffer saline solution with 5% food dye): photography of (b) yellow, green and red dye solution stopped on the valves, respectively, (c) yellow dye solution flowed after valve opened, (d) red dye solution flowed after valve opened and (e) green dye solution flowed after valve opened (ruler scale on the right side).

a portable device could reduce the risk of illness. The conventional and accepted culture methods to detect bacteria are laborious and time-consuming. Although polymerase chain reaction (PCR) can detect low concentrations of bacteria, the detection processes is complicated and the results are easily affected by sample purity. Our proposed method as well as enzyme-linked immunosorbent assays (ELISA) are commonly used immunological-based assays, which are rapid, sensitive and specific to target antigens. Electrochemical detection of *Salmonella* was performed using the microfluidic device. In order to sample larger volumes, a preconcentration step that utilizes antibody-coated magnetic beads was employed. Following concentration, the bacteria were tagged with an antibody-alkaline phosphatase reporter.[45,46] When the sandwiched analytes were deposited into the microfluidic device, the magnet under working electrode was able to capture the complex on the working electrode. The beads were washed with a buffer from the second inlet followed by the introduction of a reaction solution from the third inlet. The reaction solution contained AAP and TCEP that allow a prolonged electrochemical reaction. The ALP on reporter antibodies can catalyse AAP to produce AA, which can be regenerated by TCEP. On the working electrode, the electroactive AA can be electrochemically detected by the amperometric response (Fig. 8a). And the electron transfer rate was used to quantify the concentration of *Salmonella*. The charge on the working electrode increased linearly as time increased (Fig. 8b). The charges at 100 seconds for *Salmonella* solution (0, 10^5 and 10^6 CFU mL^{-1}) were 3.44 ± 0.66, 13.61 ± 1.49 and 33.83 ± 6.37, respectively. These concentrations of bacteria all exhibited a statistical significance among them ($P < 0.01$) (Fig. 8c). In addition, the repeatability of the device is demonstrated by the relative low standard deviation within the replicates.

Conclusions

Current fabrication methods for biosensors such as photolithography are costly and therefore can increase the cost of the final devices significantly. Low-cost methods exist for device such as lateral flow assays, but are limited in their complexity. There exists a gap in current technology for a low-cost nanofabrication method that can produce advanced biosensors in a continuous low-cost scalable manner. In order to deliver a low-cost device to users, both the materials and manufacturing methods must be accounted for. Until complex microfluidic devices can demonstrate superior function while maintaining affordability, they will remain out of the hands of potential users. By balancing the cost of manufacture and raw materials, we have fabricated a low-cost, pump-free, capillary flow-driven microfluidic chip which can control the flow of solution in the microchannels, as well as perform an electrochemical detection. The fabricating process is designed for a roll-to-roll system to obtain commercial-scale fabrication with high throughput and low-cost. The flexible microfluidic channel consisted of two layers of PET film bonded by TE polymer microfluidic channel using nanoimprint lithography.

This process was designed to mimic prototyping for roll-to-roll manufacturing. In roll-to-roll systems, gravure coating will be used in place of spin coating in order to form a thin layer of material on the PET films. Techniques such as gravure coating, nanoimprint lithography, inkjet printing and photonic curing can be paired with these roll-to-roll system to allow high throughput fabrication.[15,16,32] The results in

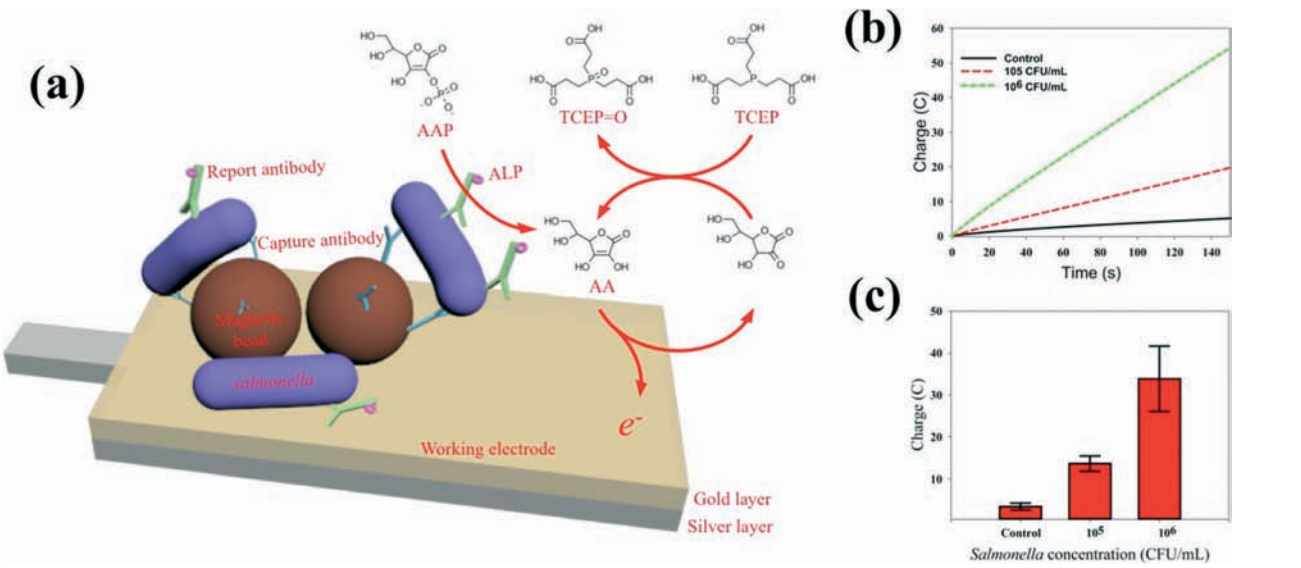

Fig. 8 (a) Schematic representation of electrochemical detection of *Salmonella* based on generation of AA by ALP on reporter antibodies and redox cycling of AA by TCEP. (b) Chronocoulograms obtained at 0.35 V on working electrode for *Salmonella* with a concentration of 0, 10^5 and 10^6 CFU mL^{-1}. (c) Concentration dependence of charge at 100 seconds on *Salmonella* (error bars represent the standard deviation of a minimum of three replicates).

this study will enable biosensors fabrication on a larger commercial scale and with high throughput in the future. The ability to fabricate cost effective biosensors using roll-to-roll system will have a significant impact on the High-Tech Nanomanufacturing industry.

Acknowledgements

Support was provided by Center for Hierarchical Manufacturing, a National Science Foundation Nanoscale Science and Engineering Center at the University of Massachusetts supported under the NSF Award Number CMMI-1025020. The authors would also like to thank Brenda Warren in the Department of Polymer Science and Engineering at the University of Massachusetts, Amherst for her assistance with inkjet printing.

Notes and references

1 K. Ren, J. Zhou and H. Wu, *Acc. Chem. Res.*, 2013, **46**, 2396–2406.
2 E. Fu, T. Liang, P. Spicar-Mihalic, J. Houghtaling, S. Ramachandran and P. Yager, *Anal. Chem.*, 2012, **84**, 4574–4579.
3 B. R. Lutz, P. Trinh, C. Ball, E. Fu and P. Yager, *Lab Chip*, 2011, **11**, 4274–4278.
4 P. Yager, T. Edwards, E. Fu, K. Helton, K. Nelson, M. R. Tam and B. H. Weigl, *Nature*, 2006, **442**, 412–418.
5 H. Varmus, R. Klausner, E. Zerhouni, T. Acharya, A. Daar and P. Singer, *Science*, 2003, **302**, 398–399.
6 N. R. Pollock, J. P. Rolland, S. Kumar, P. D. Beattie, S. Jain, F. Noubary, V. L. Wong, R. A. Pohlmann, U. S. Ryan and G. M. Whitesides, *Sci. Transl. Med.*, 2012, **4**, 152ra129.
7 E. Fu, T. Liang, J. Houghtaling, S. Ramachandran, S. A. Ramsey, B. Lutz and P. Yager, *Anal. Chem.*, 2011, **83**, 7941–7946.
8 H. Klank, J. P. Kutter and O. Geschke, *Lab Chip*, 2002, **2**, 242–246.
9 G. Lee, S. Chen, G. Huang, W. Sung and Y. Lin, *Sens. Actuators, B*, 2001, **75**, 142–148.
10 Y. Lu, W. Shi, J. Qin and B. Lin, *Anal. Chem.*, 2009, **82**, 329–335.
11 G. M. Whitesides, *Nature*, 2006, **442**, 368–373.
12 E. Sollier, C. Murray, P. Maoddi and D. Di Carlo, *Lab Chip*, 2011, **11**, 3752–3765.
13 C. F. Carlborg, T. Haraldsson, K. Oberg, M. Malkoch and W. van der Wijngaart, *Lab Chip*, 2011, **11**, 3136–3147.
14 F. Saharil, C. F. Carlborg, T. Haraldsson and W. van der Wijngaart, *Lab Chip*, 2012, **12**, 3032–3035.
15 J. John, Y. Tang, J. P. Rothstein, J. J. Watkins and K. R. Carter, *Nanotechnology*, 2013, **24**, 505307.
16 J. John, M. Muthee, M. Yogeesh, S. K. Yngvesson and K. R. Carter, *Adv. Opt. Mater.*, 2014, **2**, 581–587.
17 J. Liu, T. Pan, A. T. Woolley and M. L. Lee, *Anal. Chem.*, 2004, **76**, 6948–6955.
18 Z. Jin and N. Hildebrandt, *Trends Biotechnol.*, 2012, **30**, 394–403.
19 W. R. Jong, T. H. Kuo, S. W. Ho, H. H. Chiu and S. H. Peng, *Int. Commun. Heat Mass Transfer*, 2007, **34**, 186–196.
20 D. Bodas and C. Khan-Malek, *Microelectron. Eng.*, 2006, **83**, 1277–1279.
21 F. He, J. Grimes, S. D. Alcaine and S. R. Nugen, *Analyst*, 2014, **139**, 3002–3008.
22 T. Merian, F. He, H. Yan, D. Chu, J. N. Talbert, J. M. Goddard and S. R. Nugen, *Colloids Surf., A*, 2012, **414**, 251–258.
23 J. T. Fourkas, *J. Phys. Chem. Lett.*, 2010, **1**, 1221–1227.
24 X. Zhang, Q. Wang, B. Gablaski, X. Zhang, P. Lucchesi and Y. Zhao, *Lab Chip*, 2013, **13**, 3090–3097.
25 F. He and S. R. Nugen, *Microfluid. Nanofluid.*, 2014, **16**, 879–886.
26 C. K. W. Koo, F. He and S. R. Nugen, *Analyst*, 2013, **138**, 4998–5004.
27 W. Satoh, H. Yokomaku, H. Hosono, N. Ohnishi and H. Suzuki, *J. Appl. Phys.*, 2008, **103**, 034903.
28 H. Lorenz, M. Despont, N. Fahrni, J. Brugger, P. Vettiger and P. Renaud, *Sens. Actuators, A*, 1998, **64**, 33–39.
29 L. Libioulle, A. Bietsch, H. Schmid, B. Michel and E. Delamarche, *Langmuir*, 1999, **15**, 300–304.
30 S. R. Nugen, P. J. Asiello, J. T. Connelly and A. J. Baeumner, *Biosens. Bioelectron.*, 2009, **24**, 2428–2433.
31 F. Salam and I. E. Tothill, *Biosens. Bioelectron.*, 2009, **24**, 2630–2636.
32 D. Angmo, T. T. Larsen-Olsen, M. Jørgensen, R. R. Søndergaard and F. C. Krebs, *Adv. Energy Mater.*, 2013, **3**, 172–175.
33 J. Perelaer, M. Klokkenburg, C. E. Hendriks and U. S. Schubert, *Adv. Mater.*, 2009, **21**, 4830–4834.
34 J. Ko and H. B. Lim, *Anal. Chem.*, 2014, **86**, 4140–4144.
35 Y. H. Dou, N. Bao, J. J. Xu and H. Y. Chen, *Electrophoresis*, 2002, **23**, 3558–3566.
36 D. Maniglio, Y. Ding, L. Wang and C. Migliaresi, *Polymer*, 2011, **52**, 5102–5106.
37 L. Wang, Z. Zhang and Y. Ding, *Soft Matter*, 2013, **9**, 4455–4463.
38 S. M. Bidoki, D. M. Lewis, M. Clark, A. Vakorov, P. A. Millner and D. McGorman, *J. Micromech. Microeng.*, 2007, **17**, 967–974.
39 C. O. Laoire, S. Mukerjee, K. M. Abraham, E. J. Plichta and M. A. Hendrickson, *J. Phys. Chem. C*, 2009, **113**, 20127–20134.
40 C. F. Gonzalez, D. M. Cropek and C. S. Henry, *Electroanalysis*, 2009, **21**, 2171–2174.
41 W. Dungchai, O. Chailapakul and C. S. Henry, *Anal. Chem.*, 2009, **81**, 5821–5826.
42 J. Alvarez, M. Sota, A. B. Vivanco, I. Perales, R. Cisterna, A. Rementeria and J. Garaizar, *J. Clin. Microbiol.*, 2004, **42**, 1734–1738.
43 K. Ohtsuka, K. Yanagawa, K. Takatori and Y. Hara-Kudo, *Appl. Environ. Microbiol.*, 2005, **71**, 6730–6735.
44 J. Chen, Z. Jiang, J. D. Ackerman, M. Yazdani, S. Hou, S. R. Nugen and V. M. Rotello, *Analyst*, 2015, DOI: 10.1039/C5AN00637F.

45 M. R. Akanda, M. A. Aziz, K. Jo, V. Tamilavan, M. H. Hyun, S. Kim and H. Yang, *Anal. Chem.*, 2011, **83**, 3926–3933.

46 M. R. Akanda, V. Tamilavan, S. Park, K. Jo, M. H. Hyun and H. Yang, *Anal. Chem.*, 2013, **85**, 1631–1636.